EasyChair Preprint

№ 6570

A PIV Experiment of Water Jet Through a Single Nozzle at Bottom Hole

Heqian Zhao, Zhongwei Huang, Huaizhong Shi, Zhenliang Chen, Ziang Gu and Fei Gao

September 13, 2021

Proceedings of the 48th National Conference on Fluid Mechanics and Fluid Power (FMFP)
December 27-29, 2021, BITS Pilani, Pilani Campus, RJ, India. (TNR 10 Bold)

FMFP2021–XX–YYY

A PIV Experiment of Water Jet through a Single Nozzle at Bottom Hole

ABSTRACT

Hydraulics mechanics is significantly important in the drilling process of oil or gas exploration, especially for the drill bit. The fluid flows through the nozzles on the bit and generates a water jet to remove the cutting at the bottom hole. In this paper, a simplified bottom hole model is established. The Particle Image Velocimetric (PIV) is used to capture the flow field of the single nozzle. Due to the limitation of the bottom and wellbore, the potential core is shorter than that of the free water jet. The velocity magnitude rapidly attenuates when fluid close to the bottom is lower than about 5 mm. Besides, a vortex zone appears near the middle of the bottom beside the water jet zone. A modified exponential function can be used to fit the centerline velocity well. On the one hand, the results of this paper can provide verification for the numerical simulation of the bottom hole flow field. On the other hand, it also can provide an experimental basis for the hydraulic design of the drill bit.

Keywords: Oil and gas, Hydraulic mechanic of drilling, PIV, Bottom hole, Refractive index compensation

1. INTRODUCTION

Nowadays, oil and natural gas are still one of the major energy sources in the world. Drilling is an essential link in oil and gas development. During the drilling process, the drill bit is used to break the rock at the bottom hole. The drilling fluid flows through the pipe and nozzles to generate a water jet. On the one hand, the water jet removes the cuttings to keep a clean bottom hole and annual. On the other hand, the water jet erodes the bottom of the hole in soft formations to improve the rate of penetration[1]. However, the drill bit flow field is extremely complex. And few papers are focus on this research area. Therefore, it is necessary to conduct more studies on the flow field of the bit at the bottom hole.

2. LITERATURE REVIEW AND OBJECTIVE

The PIV is a non-contact flow field measurement system, which is widely used for single-phase or multi-phase fluid flow field measurement and analysis[2-5]. At the same time, the system resolves many problems for water jet measure and is widely used. Milanovic[6] studied the near-field region of a turbulent round jet. Lee[7] used the proper orthogonal decomposition (POD) method to analyze the jet fusion characteristics of double nozzles. The submerged water jet at high-pressure ambient conditions was also conducted using the PIV system[8-10]. The dual-jet flow field[11], high-speed pulsating water jets[12], and impinging jets [13] were also be measured.

Refractive index compensation is an important step in the PIV experiment. The optimal result should be that all objects in the experiment can achieve index matching[14]. However, it is not easy to achieve. Many kinds of fluids are adopted as a refractive matching or compensating fluid[15], such as phenyl silicone oil[2], the aqueous solution of NaCl and sucrose[3], P-Cymene[16], the NaI solution[17], et al.

Radenko Drakulic introduced the PIV in the drill bit flow field measurement[1, 18]. However, the relative results are not enough to support the hydraulic design for the drill bit. Therefore, a simplified PIV test under bottom hole conditions is carried out in this paper.

In this paper, a simplified bottom hole condition is established using the similarity criterion[19-23]. A single nozzle flow field is captured by PIV system. The transparent wellbore and pipe are made of plexiglass. The refractive compensation is adopted to reduce the laser reflection of the wellbore. Based on the flow field characteristics of a sinlge-nozzle water jet at the bottom hole, we analyze the influence of nozzle diameter and flow rate on the flow field.

3. Experimental set-up

The flow field of water jet through nozzles at the bottom hole is investigated experimentally. The overview of the experimental facility and the PIV system is presented in Fig. 1. The closed-loop system is comprised of a water tank, centrifugal pump, valves, turbine flow meter, and plexiglass wellbore. The water flows through the loop delivered by the centrifugal pump with an 8 m^3/h capacity and 16 m head of delivery and is discharged into the water tank. The flow rate of nozzles is controlled by a valve combination. There are two valves in the combination. One of the valves is installed in the backbone of the tube, and the other is in the branch as a throttle valve. The range of the turbine flow meter is 1-10 m^3/h with the ±0.5% nominal accuracy.

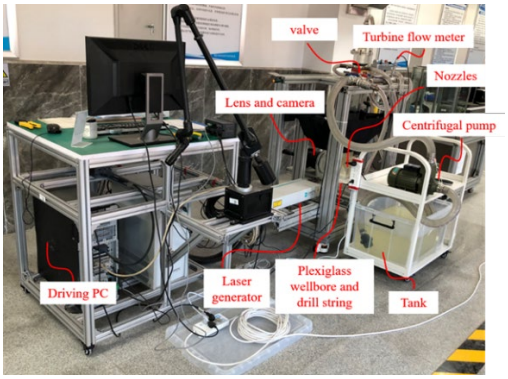

Figure 1: The overview of the experimental facility with PIV system.

The plexiglass wellbore is 1000 mm long with a 100 mm diameter. The thickness of the wellbore wall is approximately 10 mm. A plexiglass drill pipe combined with nozzles is instilled in the wellbore. There is a 16 mm gap between the wellbore and drill pipe. As shown in the figure, the plexiglass wellbore is surrounded by a rectangular plexiglass sink. During the experiment, one of the refractive index compensation fluids is filled in the sink. The refractive index compensation fluid can reduce the reflected laser of the wellbore. The laser generator and charge-coupled device (CCD)camera are installed perpendicular to the plexiglass sink wall, respectively. A laser sheet issued by the laser generator will illuminate the tracking particles. The scattered laser will be captured by the CCD camera.

The laser source is an Nd: YAG double-pulse laser with a repetition rate of 15 Hz, which can generate a 532 nm, 135mJ dual-pulse laser. The capture system is composed of a 14 bit 2048 × 2048 pixels CCD camera and a telecentric lens. The telecentric lens is not sensitive to the focal length and is suitable for shooting in the flow field with a large depth of field. The silver-coated hollow glass spheres (S-HGS) were used as the tracking particles in this experiment. The diameter and density of the S-HGS are 10 μm and 1.40 g/cm^3, respectively.

The refractive index compensation fluid is filled in the rectangular plexiglass sink to reduce the reflected laser of the wellbore. As the pre-experiment, the refractive index of fluids and plexiglass are measured using the abbe refractometer. The refractive index of plexiglass of wellbore and sink is about 1.48687. Therefore, the 100 # white oil, whose average refractive index is 1.4858, is used as the refractive compensating fluid.

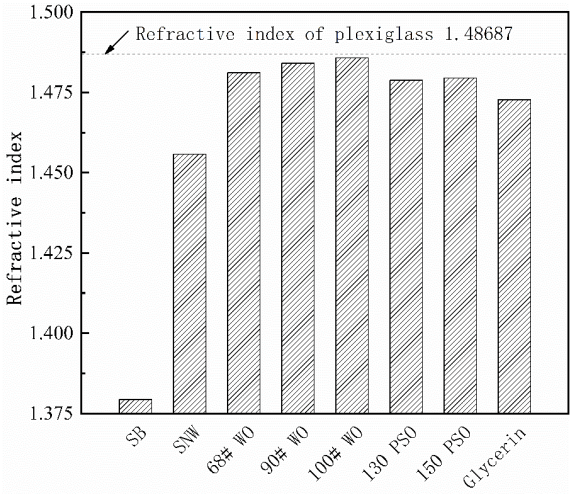

Figure 2: The refractive index of fluids (SB- Saturated brine, SNW- Sucrose + NaCl + water, 68# WO- 68# White Oil, 100# WO-100# White Oil, 130 PSO-Phenyl silicone oil with a kinematic viscosity of 130 cs, 150 PSO-Phenyl silicone oil with a kinematic viscosity of 150 cs)

4. Experimental set-up

In the oil and gas drilling process, a polycrystalline diamond compact (PDC) drill bit usually has 3 to 7 nozzles. The size of each nozzle is 14 mm to 24 mm. However, considering the difference in flow rate between the field and experiment, the size of the nozzle of experiments is scaled using the similarity criterion[19-23]. The geometric similarity criterion, which is widely adopted in the laboratory experiment[20], is used to determine the size of the nozzle in the experiment. The geometric similarity is defined that the model is the same shape as the application, usually scaled. The experimental nozzle size is specified depending on the wellbore size ratio in the actual drilling process and experiment. Eq. (1) shows the geometric similarity.

$$\frac{D_{w_{\text{actual}}}}{D_{w_{\text{experiment}}}} = \frac{D_{N_{\text{actual}}}}{D_{N_{\text{experiment}}}} \quad (1)$$

where D_w and D_N are the diameters of wellbore and nozzle, the indexes of actual and experiment mean the actual drilling and experimental conditions. The size of the experimental nozzles is shown in Table 1. The eventual size of nozzles is designed as 6, 8, 10, and 12 mm.

Table 1: The size of experimental nozzles

No.	Actual drilling process		Experimental condition	
	Wellbore size, mm	Nozzle size, mm	Experimental wellbore size, mm	Experimental nozzle size, mm
1	215.9	14	100	6.5
2	215.9	16	100	7.4
3	215.9	18	100	8.3
4	215.9	20	100	9.3
5	215.9	22	100	10.2

6	215.9	24	100	11.1

The flow rate of the experiment is specified based on the dynamic similarity[23]. The Reynolds number is adopted to describe the dynamic similarity of the experiment. The density and viscosity of drilling fluid are in an extensive range. In this experiment, the density and viscosity are chosen 1.2 g/cm^3 and 10 mPa·s, respectively. The experimental fluid is water, whose density and viscosity are 1 g/cm^3 and 1 mPa·s, respectively.

$$\mathrm{Re} = \frac{\rho d v}{\mu} \tag{2}$$

where ρ, d, v are the density, characteristic length, and characteristic velocity of the flow field at the bottom hole. The flow rate of the experiment is designed as 0.80, 0.96, 1.12, and 1.28 m^3/h, which is corresponding to 20 L/s to 32 L/s (72 m^3/h to 115.2 m^3/h) for actual drilling. The Reynolds number is more than 6,00,00 when water jets through a single nozzle from the Eq. (2).

Table 2: The arrangement of the experiment

No.	Nozzle diameter, mm	Nozzle angle, °	Distance to bottom, mm	Flow rate, m^3/h
1	6	20	17	1.28
2	8			0.80/0.96/ 1.12/1.28
3	10			1.28
4	12			1.28

5. RESULTS AND DISCUSSION

One of the original images of a water jet through a single nozzle is demonstrated in Fig. 3. Due to the different flow rates, the time interval between the two recordings is not identical. The time between the laser pulses is set in the range of 60 μs to 80 μs. For PIV analysis, the final interrogation area (IA) is 32 × 32 pixels with a 75% overlap in horizontal and vertical directions. An initial IA of 64 × 64 pixels is sequentially reduced to the final IA. During each iteration cycle, a local comparison of vector attributes with the median value of 9 × 9 neighbors is used to validate and remove outliers. A minimum peak height ratio of 1.1 is used to remove spurious vectors[6].

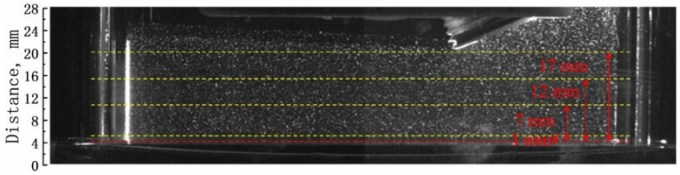

Figure 3: The original image of water jet through a single nozzle

An adaptive cross-correlation method is adopted to evaluate the velocity field determined from each pair of particle images, using mentioned parameters. The streamline of the instantaneous flow field is shown in Fig. 4. The water jets through the nozzle and forms a strong and complex turbulent flow field. The jet structure has a wide gap between the bottom hole and the free water jet[6, 8]. The water jet flows bake after impinging the bottom. In addition, due to the impinging angle of the water jet, the crossflow generated by the jet is not symmetrical[13]. The instantaneous flow field fluctuates extremely, as shown in Fig. 4. However, the vortex and water jet domain is evident in the instantaneous flow field. At each measurement, 50 images are obtained and used to evaluate the mean flow field and for other analyses.

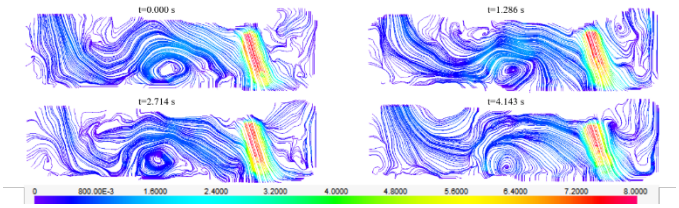

Figure 4: The streamline of the instantaneous flow field with the 6 mm nozzle (flow rate = 1.12 m3/h)

5.1 The effection of nozzle diameter on flow field characteristics

Compare the contour map of the time-averaged velocity field with different diameters nozzles when the flow rate is 1.28 m^3/h with the nozzles is 17 mm to bottom, as illustrated in Fig. 5. The water through the nozzle generates a high-velocity jet. The water jet has a potential core beneath the nozzle. Limited by the bottom and the wellbore, the jet deviates from the centerline along the bottom and forms a crossflow. It is obvious that the smaller nozzle forms a higher-velocity jet at the same flow rate. In contrast, the width of the jet is reduced. The contour lines are dense on both sides of the jet, which indicates that the jet boundary has a large velocity gradient. This also generates a high shear rate between the water jet and surrounding fluid, which causes the surrounding fluid to flow.

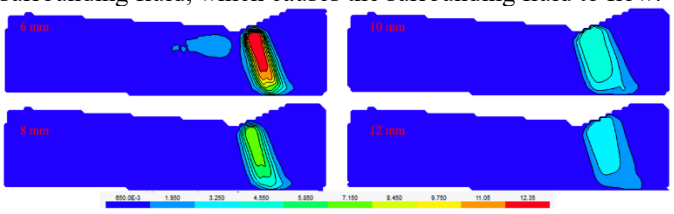

Figure 5: The contour map of the velocity field with different diameters nozzle (flow rate = 1.28 m^3/h)

The most important roles of the jet in drilling are effectively removing the cuttings at the bottom to keep the hole clean and eroding the bottom of the hole in soft formations, respectively[1]. The potential core contains most of the hydraulic energy of the water jet, which is paid more attention to during the drilling process. For a free water jet, the potential core is usually defined as the domine that the centerline velocity is over 95% of the jet exit velocity V_{max} [8]. In this experiment, the potential core is defined as the area whose velocity is over 80% of the V_{max}, due to the water jet is significantly obstructed by the boundary[1]. The centerline velocity of different nozzles with the flow rate of 1.28 m^3/h is illustrated in Fig. 6. It is evident to observe the potential core, although the water jet is

obstructed by the boundary. The velocity remains stable firstly beneath the nozzle then decreases rapidly as fluid approaches the bottom. The velocity stability section contains the potential core. The length of the potential core (V > 80 % V_{max}) is statistics, as shown in Fig. 7. Due to the velocity data along the centerline is dispersed, there is an uncertainty interval whose velocity range contains the 80 % V_{max}. And the zone in which the fluid velocity is lower than 80 % V_{max} is the attenuation zone. It has a higher velocity gradient in the attenuation zone. It found that the potential core length is shorter than that of the free water jet whose potential core is about 4-6 diameter of the nozzle[6, 7]. The velocity magnitude rapidly attenuates when fluid close to the bottom is lower than about 5 mm.

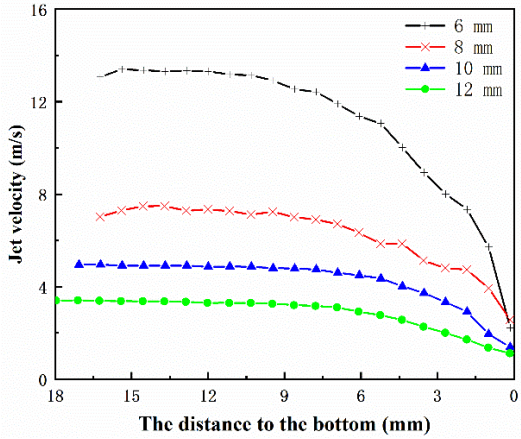

Figure 6: The centerline velocity profiles of different nozzles(flow rate = 1.28 m³/h)

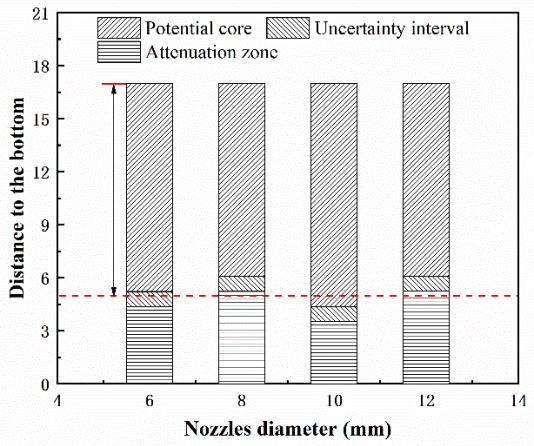

Figure 7: The potential core of different nozzles(flow rate = 1.28 m³/h)

The dimensionless velocity, V/V_{max}, is used to find the relationship between the velocity and the distance to the bottom. As illustrated in Fig 8, the dimensionless velocity data of different diameter nozzles evolves to an identical trend. This evolution reflects the self-modeling of the water jet. A modified exponential function is used to fit all of the data. The fitted function is shown in Eq. (3). The coefficient of determination between the fitting curve and experimental data is about 0.913.

$$\frac{V}{V_{max}} = 0.97729\left(1-e^{-0.4116x}\right) \quad (3)$$

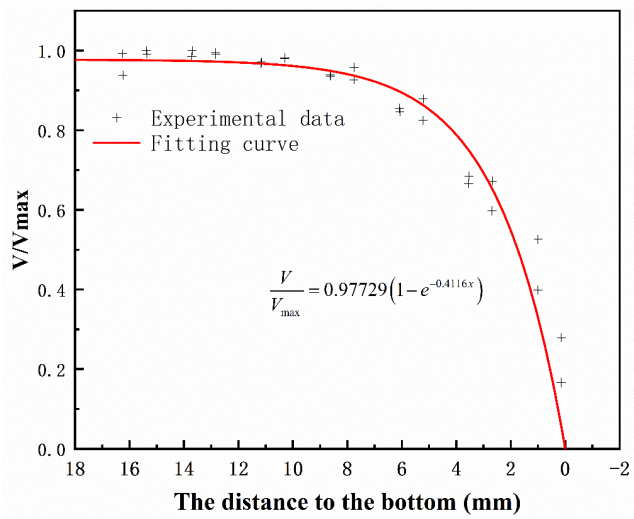

Figure 8: The relationship between dimensionless velocity and the distance to the bottom (flow rate = 1.28 m³/h)

The time-averaged streamline of the flow field of different diameter nozzles is presented in Fig. 9. The time-averaged streamline is more regular than the instantaneous streamline in Fig. 4. Compared with the contour map in Fig. 5, it is easy to find the vortex domain and water jet domain in the streamline diagram. Near the middle of the bottom, a vertex is formed. A set of the streamline is surrounding the vortex. The streamline with the flow direction of 8mm nozzles is illustrated in Fig. 10 as an example. Due to the entrainment of the water jet, the fluid around the jet is carried and accelerated[24-26]. The ultimate velocity direction is the same as the water jet. However, the fluid near the vortex, which is not adjacent to the jet, flows towards the jet. The streamline of fluid, which is mentioned above, wraps the vortex. The streamline attaches to the bottom and then separates. This phenomenon may create another crossflow on the other side of the vortex. The particles tend to be distributed at the edge of the vortex[27]. If a single nozzle with 20 ° is installed at the bottom hole during drilling, the cuttings may be removed and distributed near the vortex. However, the vortex may cause the cuttings to obstruct at the bottom.

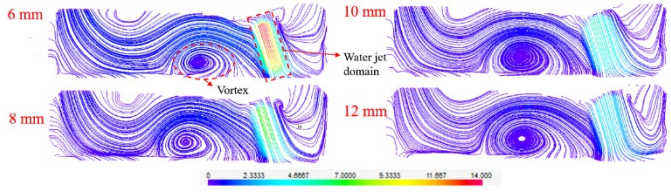

Figure 9: The streamline of the flow field with different nozzle diameters (flow rate = 1.28 m³/h)

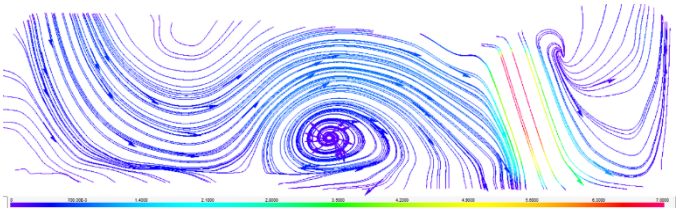

Figure 10: The streamline with the flow direction of 8mm nozzle (flow rate = 1.28 m³/h)

5.2 The effection of flow rate on flow field characteristics

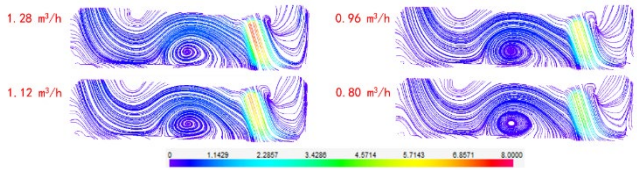

Figure 11: The streamline of the flow field with different flow rates (8 mm nozzle)

The streamline of the flow field with different flow rates is presented in Fig. 12, which is corresponding to case 2. When the flow rate increases from 0.8 m^3/h to 1.28 m^3/h, the streamline has no significant changes except the water jet velocity. The centerline velocity of the 8 mm nozzle with different flow rates is plotted at the same time. The potential cores at different flow rates have the same length. When the distance to the bottom is lower than about 6 mm, the fluid velocity reduces rapidly. The fitting relationship between the dimensionless velocity and distance to the bottom is in Eq. (4).

$$\frac{V}{V_{\max}} = 0.95792\left(1-e^{-0.40936x}\right) \quad (4)$$

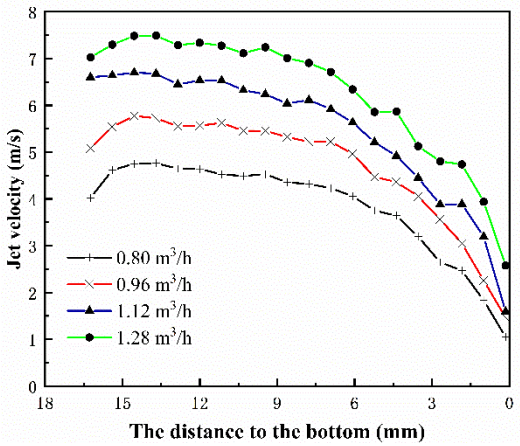

Figure 12: The centerline velocity profiles of different flow rates (8 mm nozzle)

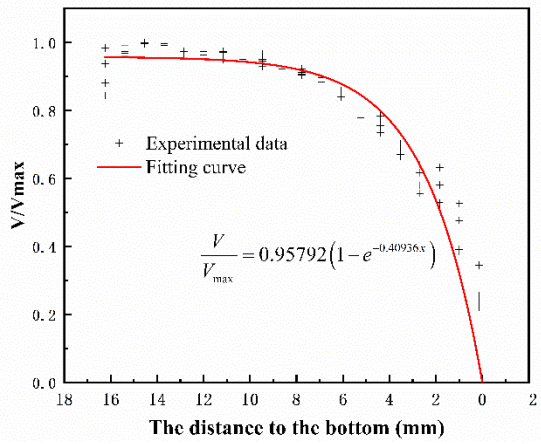

Figure 13: The relationship between dimensionless velocity and distance (8 mm nozzle)

6. CONCLUSIONS

In this paper, a simplified bottom hole model is established, and a PIV system is used to capture the flow field of the single nozzle. The refractive compensation is adopted to reduce the laser reflection of the wellbore. From the results, we can conclude:

(1) The 100 # white oil, whose average refractive index is 1.4858, can be used as the refractive compensating fluid for plexiglass wellbore.
(2) The flow field of the single nozzle at the bottom hole can be divided into vortex zone and water jet zone.
(3) The potential core of the water jet limited by bottom and wellbore is shorter than that of the free water jet.
(4) The fluid velocity reduces rapidly when fluid close to the bottom is lower than about 5 mm.

ACKNOWLEDGEMENTS

This study is supported by the Strategic Cooperation Technology Projects of CNPC and CUPB (ZLZX2020-01)

NOMENCLATURE

$D_{wactual}$	Diameters of the wellbore during drilling	[m]
$D_{wexperiment}$	Diameters of the wellbore of experiment	[m]
$D_{Nactual}$	Diameters of the nozzle on the drill bit	[m]
$D_{Nexperiment}$	Diameters of nozzle of the experimet	[m]
V	The velocity of the fluid	[m/s]
V_{max}	The water jet velocity	[m/s]
Re	Reynolds number	--
ρ	The density of the fluid	[kg/m³]
d	The characteristic length	[m]
v	The characteristic velocity	[m/s]

REFERENCES

[1] Drakulic R, Grant I. The Application of Particle Image Velocimetry (PIV) and Laser Doppler Velocimetry (LDV) in the Study of Drilling Bit Nozzles. IADC/SPE Drilling Conference: OnePetro; 1994.

[2] Li G, Gao Z, Li Z, Wang J, Derksen J. Particle-resolved PIV experiments of solid-liquid mixing in a turbulent stirred tank. AIChE Journal. 2018;64:389-402.

[3] Li G, Li Z, Gao Z, Wang J, Bao Y, Derksen J. Particle image velocimetry experiments and direct numerical simulations of solids suspension in transitional stirred tank flow. Chemical Engineering Science. 2018;191:288-99.

[4] Fernández ME, Pugnaloni LA, Sánchez M. Proppant transport in a planar fracture: Particle image velocimetry. Journal of Natural Gas Science and Engineering. 2021;89:103860.

[5] Simiano M, Zboray R, de Cachard F, Lakehal D, Yadigaroglu G. Advanced processing of gas-liquid PIV measurements in 3D bubble plume.

[6] Milanovic IM, Hammad KJ. PIV study of the near-field region of a turbulent round jet. Fluids Engineering Division Summer Meeting2010. p. 1353-61.
[7] Lee S, Hassan YA. Experimental study of flow structures near the merging point of two parallel plane jets using PIV and POD. International Journal of Heat and Mass Transfer. 2018;116:871-88.
[8] Jasper S, Hussong J, Lindken R. PIV investigation of high Reynolds number submerged water jets at high-pressure ambient conditions. Experiments in Fluids. 2021;62:1-15.
[9] Jasper S, Gradzki DP, Bracke R, Hussong J, Petermann M, Lindken R. Nozzle Cavitation and Rock Erosion Experiments Reveal Insight into the Jet Drilling Process. Chemie Ingenieur Technik. 2021.
[10] Jasper S, Wittig V, Lindken R. Laser optical investigation of high-pressure water jets in submerged reservoir type conditions used for high-pressure jetting. European Geothermal Congress The Hague2019.
[11] Gensheng L, Jian S, Zhongwei H, Jilei N, Can Y. An experimental study on dual jet flow with PIV method. American waterjet conference: Houston, Texas; 2005. p. 120-5.
[12] Zelenak M, Foldyna J, Scucka J, Hloch S, Riha Z. Visualisation and measurement of high-speed pulsating and continuous water jets. Measurement. 2015;72:1-8.
[13] Khayrullina A, van Hooff T, Blocken B, van Heijst G. PIV measurements of isothermal plane turbulent impinging jets at moderate Reynolds numbers. Experiments in Fluids. 2017;58:31.
[14] Wright SF, Zadrazil I, Markides CN. A review of solid–fluid selection options for optical-based measurements in single-phase liquid, two-phase liquid–liquid and multiphase solid–liquid flows. Experiments in Fluids. 2017;58:1-39.
[15] Dijksman JA, Rietz F, Lőrincz KA, van Hecke M, Losert W. Invited article: Refractive index matched scanning of dense granular materials. Review of Scientific Instruments. 2012;83:011301.
[16] Dominguez-Ontiveros E, Estrada-Perez C, Hassan Y, Banner B, Ortíz-Villafuerte J. PIV Measurements in a Matched Refractive Index Packed Bed. Transactions of the American Nuclear Society. 2005;93:399-400.
[17] Xu Y, Wang J-g, Zhao S-l, Bai Z-s. PIV experimental study on the flow field in the rotor zone of an annular centrifugal contactor. Chemical engineering research and design. 2015;94:691-701.
[18] Drakulić R, Steiner I, Krištafor Z. THE APPLICATION OF LASERS IN MEASUREMENT OF FLUID FLOW THROUGH DRILLING BIT NOZZLES. Rudarsko-geološko-naftni zbornik. 1993;5:201-8.
[19] Chanson H. Hydraulics of open channel flow: Elsevier; 2004.
[20] Chanson H. Turbulent air–water flows in hydraulic structures: dynamic similarity and scale effects. Environmental fluid mechanics. 2009;9:125-42.
[21] Chaudhry MH. Open-channel flow: Springer Science & Business Media; 2007.
[22] Sedov LI, Volkovets A. Similarity and dimensional methods in mechanics: CRC press; 2018.
[23] Tropea C, Yarin AL, Foss JF. Springer handbook of experimental fluid mechanics: Springer; 2007.
[24] Guha A, Barron RM, Balachandar R. An experimental and numerical study of water jet cleaning process. Journal of Materials Processing Technology. 2011;211:610-8.
[25] Han D, Mungal M. Direct measurement of entrainment in reacting/nonreacting turbulent jets. Combustion and flame. 2001;124:370-86.
[26] Ho C-M, Gutmark E. Vortex induction and mass entrainment in a small-aspect-ratio elliptic jet. Journal of Fluid mechanics. 1987;179:383-405.
[27] Jafari S, Salmanzadeh M, Rahnama M, Ahmadi G. Investigation of particle dispersion and deposition in a channel with a square cylinder obstruction using the lattice Boltzmann method. Journal of Aerosol Science. 2010;41:198-206.